




Atomic disorder in Ni-V alloys studied using neutron scatteringAdane Gebretsadik ^{1,*}, Ruizhe Wang,¹ Arwa Alyami,¹ Hind Adawi ^{1,2}, Jean-Guy Lussier,¹
Katharine L. Page,^{3,4} and Almut Schroeder ^{1,†}¹*Department of Physics, Kent State University, Kent, Ohio 44242, USA*²*Department of Physics, Jazan University, Jazan 45142, Kingdom of Saudi Arabia*³*Spallation Neutron Source, Oak Ridge National Laboratory, Oak Ridge, Tennessee 37831, USA*⁴*Department of Materials Science and Engineering, The University of Tennessee, Knoxville, Tennessee 37996, USA*

(Received 14 March 2023; revised 31 August 2023; accepted 1 November 2023; published 20 November 2023)

We present a pair distribution function (PDF) analysis from neutron diffraction data of the $\text{Ni}_{1-x}\text{V}_x$ alloy in the Ni-rich regime. Such structural study aims to clarify the origin of the magnetic inhomogeneities associated with the quantum Griffiths phase close to the ferromagnetic-paramagnetic quantum phase transition. The PDF analysis successfully reveals information about structural and atomic disorder comparing short-range correlations in our $\text{Ni}_{1-x}\text{V}_x$ polycrystalline samples prepared with high-temperature annealing and rapid cooling protocol. This study confirms the expectations that all $\text{Ni}_{1-x}\text{V}_x$ samples with $0 \leq x \leq 0.15$ crystallize in a single phase fcc structure with some residual strain. The lattice constant and the atomic displacement parameter increase with V concentration x . Both changes are consistently explained by a random occupation of V and Ni atoms on the lattice sites with small displacements due to the different atomic radii with ratio (r_V/r_{Ni}) of 1.05. Probing alternate, simple models of the local PDF, such as V clusters or ordered structures (Ni_8V , Ni_3V), gives inferior results compared to a random occupation. This investigation strongly supports the magnetic clusters in the binary alloy $\text{Ni}_{1-x}\text{V}_x$ originating from Ni-rich regions created from *random* occupation rather than from chemical clusters. The simple tests already demonstrate that $\text{Ni}_{1-x}\text{V}_x$ is one of the rare examples of a solid solution in a wide concentration regime (up to $x = 0.15$) persisting down to low temperatures ($T = 15$ K).

DOI: [10.1103/PhysRevB.108.184106](https://doi.org/10.1103/PhysRevB.108.184106)**I. INTRODUCTION**

Ni alloys remain highly attractive materials for their tunable mechanical and magnetic properties. While pure Ni is a very weak ductile metal forming a simple fcc lattice, small amounts of defects typically increase the mechanical strength. Already in a binary alloy partial substitution of Ni by another d electron element X allows for the formation of partially ordered structures that modify the mechanical properties. Ni superalloys [1] containing local ordered structures within an occupational disordered Ni matrix with defects are well known for high-temperature applications. Also, multicomponent alloys [2] of similar $3d$ elements ranging from Cr to Ni, called high entropy alloys [3], are promising materials for their increased mechanical strength. The individual local Ni environment and small lattice variations play an essential role. More sophisticated structural methods [4] beyond the traditional diffraction techniques are required to resolve local deviations and short-range order [5].

The same is true for the magnetic properties. On the one hand, Ni is one of the few elemental ferromagnets (FM) with a high critical temperature $T_c = 630$ K [6], while on the other hand the magnetism of Ni is very sensitive to changes in the local environment caused by other elements that weaken the

magnetic moment and the magnetic order. It is known that T_c is easily tuned [7,8] in $\text{Ni}_{1-x}\text{X}_x$ by partial chemical substitution of Ni with another d element X down to very low values. Ni alloys seem to provide a good opportunity for observing magnetic quantum phase transitions (QPT) by reducing the FM ordering temperature T_c down to zero and leaving a paramagnetic phase (PM) without magnetic order. Various binary alloys have been studied, which show a suppression of T_c toward zero by varying the composition x . Different critical concentrations x_c are extrapolated depending on $3d$ or $4d$ element X [7,9]: e.g., X = Cr, V with $x_c \approx 0.12$, X = Rh, Cu, Pt with $x_c \approx 0.4$ – 0.6 , and X = Pt with $x_c \approx 0.95$. But the observation of any magnetic quantum critical behavior close to $T_c = 0$ is not straightforward. While partial chemical substitution is known to be an effective tuning parameter to apply chemical pressure or for electronic doping to drive through a QPT, it might modify the critical behavior by introducing *disorder* through local atomic and structural inhomogeneities. The effect of disorder is quite apparent in itinerant ferromagnets: *clean*, i.e., ideally defect-free, homogeneous FM QPT and *disordered* FM QPT are distinctly different [10]. Already the prominent $\text{Ni}_{1-x}\text{Pd}_x$ [11] with only weak disorder does not follow the prediction of a *clean* FM [10]. Strong disorder might destroy the transition, but under the right circumstances disorder can produce a new exotic quantum critical point [12] where finite size magnetic clusters play a role. Such novel quantum critical results can only be observed in magnetic alloys which present the proper distribution of random

*Present address: Intel Corp, Chandler, Arizona 85226, USA.

†aschroe2@kent.edu

magnetic clusters produced by random defects. Therefore, the full characterization of a disordered magnetic QPT includes a close look at the origin of the disorder. This study probes how *ideal disorder* can be realized in a sample by checking for random static defects.

We focus here on the alloy $\text{Ni}_{1-x}\text{V}_x$ which shows indications of a disordered magnetic QPT [13,14]. Ni-V with a very small critical concentration x_c also promises the best atomic structure, a solid solution, an fcc lattice with *random* atomic occupation. We aim to confirm this with the present study. The local atomic positions of V atoms are relevant for the magnetic QPT because only the other Ni atoms seem responsible for the magnetism. Magnetic clusters are the main signature of a disordered QPT [12,15]. So far, magnetization measurements and internal field measurements through μSR have revealed evidence for such magnetic clusters in $\text{Ni}_{1-x}\text{V}_x$ in both the PM and FM phase [14] close to x_c . It is a challenge to reveal more details of these magnetic clusters; the size distribution and dynamics range are not fully resolved. Recent small angle neutron scattering data give some size estimates [16]. However, the ideal prerequisite for random distribution of magnetic clusters are random V occupations. Any other atomic placement would modify the magnetic cluster distribution and the magnetism.

Even if an fcc lattice with random occupation is ideally predicted for Ni-rich alloys, a thorough structural investigation is essential to reveal any crystalline or chemical defects of the real Ni-V samples that might affect the magnetism. It is well known that the actual chemical structure formation of these binary alloys depends on growth conditions and post-annealing treatments (see, e.g., in Ni-Cu [17]). Different atomic arrangements, ranging from vanadium clusters to chemically ordered structures, are possible presenting different local Ni-V environments. We chose wide angle neutron diffraction to extract the local pair distribution function (PDF) [4] of our polycrystalline samples to check for deviations from the ideal structure and the ideal random chemical occupations. This method had been already successful in distinguishing order from occupational disorder [18] in a similar binary compound Cu_3Au and in recognizing the effect of short-range order. The neutron probe allows the study of larger polycrystals and offers the advantage of a high contrast between the Ni and V nuclear cross section. [The thermal coherent cross sections are $\sigma(\text{Ni}) = 13.3$ barn, $\sigma(^{58}\text{Ni}) = 26.1$ barn, and $\sigma(\text{V}) = 0.018$ barn]. Essentially, we are probing the Ni-Ni correlation expecting distinct differences in the PDF peak intensities of the first neighbors for different V occupations. To better study the direct V environment and location for close distances an x-ray PDF study becomes essential that requires a small amount of powder samples. Note that this technique does not reveal *magnetic* correlations in our FM samples; the magnetic moment contribution is too small to be resolved [$\mu(x_c) \approx 0.02 \mu_B$].

In this paper we present the first results of an atomic pair distribution function (PDF) analysis from a wide angle neutron scattering experiment that answers the main questions. The PDF method characterizes well the local chemical environment in our $\text{Ni}_{1-x}\text{V}_x$ samples (with $x \leq 0.15$) using simple models within PDFGUI [19]. It reveals that the Ni-V data are best described by a pure fcc crystal structure with the expected average Ni environment of a randomly occupied

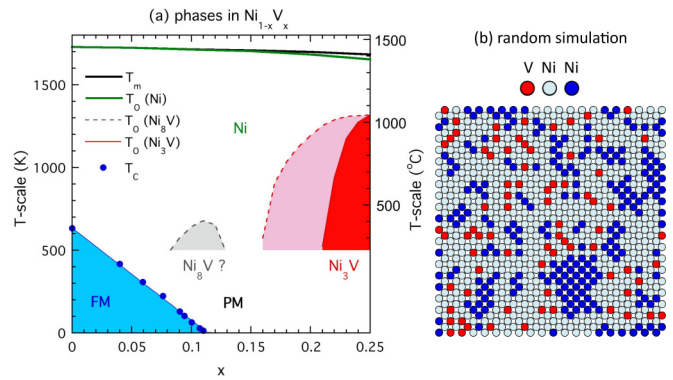


FIG. 1. (a) Structural and magnetic phase diagram of $\text{Ni}_{1-x}\text{V}_x$ (after [14,24]): the melting temperature (T_m); the onset of fcc lattice with random atomic distribution at $T_o(\text{Ni})$, of ordered Ni_3V structure at $T_o(\text{Ni}_3\text{V})$, of potential Ni_8V structure at $T_o(\text{Ni}_8\text{V})$, and the magnetic transition at T_c from paramagnetic (PM) to ferromagnetic (FM) phase are shown vs V concentration x . (b) Simulation of random atomic distribution of $\text{Ni}_{0.9}\text{V}_{0.1}$ in xy plane of fcc lattice: the red circles indicate the random occupation of V. The magnetic response of Ni depends on the neighborhood and is weaker for Ni (in light blue) with adjacent V. The other Ni (in dark blue) mainly contribute to magnetic order or form random magnetic clusters.

lattice. Comparing the fit quality of different models we can exclude large V clusters and long-range ordered atomic structures in $\text{Ni}_{1-x}\text{V}_x$ up to $x = 0.15$.

II. EXPERIMENTAL DETAILS

Polycrystalline spherical samples of $\text{Ni}_{1-x}\text{V}_x$ with V concentrations $x = 0$ to 0.15 were prepared by arc melting from high purity elements (Ni 99.995%, ^{58}Ni 99.9%, and V 99.8%), annealed in an evacuated sealed quartz tube at 1000 °C for 3 days, cooled rapidly (>200 °C/min), and investigated by several methods as described in Refs. [13,20]. The samples with $x = 0.110$ and $x = 0.123$ were made with the pure isotope ^{58}Ni and annealed at 1050 °C. Neutron diffraction data of several samples with different V concentrations x were collected at the NPDF instrument [21] at the Los Alamos Neutron Science Center. For this experiment 15–36 pellets with diameter 3–4 mm were measured for each x inside an aluminum can of diameter 3/8 in. at 15 K for 2–3 h. Also, a powder sample with $x = 0.150$ was investigated at the NOMAD instrument [22] at the Spallation Neutron Source (SNS) at the Oak Ridge National Laboratory (ORNL). The powder (~ 0.3 g) was filled inside a glass tube of 2 mm diameter and data were collected for 2 h at 300 K. The NPDF data were reduced with PDFgetN [23] (with $Q_{\text{max}} = 40 \text{ \AA}^{-1}$) to produce the total pair distribution function (PDF) in the form $G(r)$ ready to be modeled with the PDFGUI software [19]. The NOMAD data were reduced and transformed (with $Q_{\text{max}} = 31.41 \text{ \AA}^{-1}$) using the automatic data reduction scripts at the NOMAD beamline.

III. PHASE DIAGRAM OF $\text{Ni}_{1-x}\text{V}_x$

The binary alloy $\text{Ni}_{1-x}\text{V}_x$ features an apparently simple phase diagram as shown in Fig. 1(a). The ferromagnetic

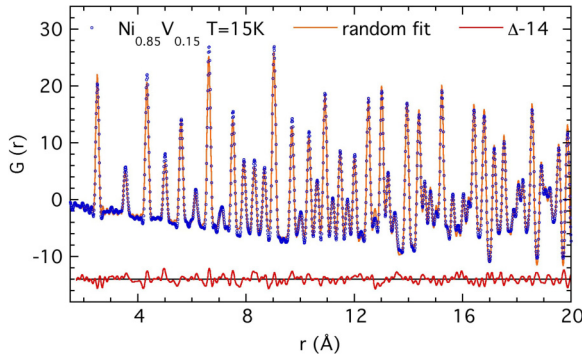


FIG. 2. Pair distribution function $G(r)$ vs pair distance r of $\text{Ni}_{0.85}\text{V}_{0.15}$ pellet data (blue circles) taken at 15 K at NPDF with random fit (orange line). The difference, $\Delta = \text{data} - \text{fit}$, is shown as a red line shifted by 14 units with residual $Rw = 11.0\%$.

ordering temperature T_c is initially linearly suppressed with increasing V concentration x , reaching zero toward $x_c = 0.116$ [13]. Signs of magnetic clusters [13,14] are found around x_c in between $x = 0.09$ and $x = 0.15$. V differs from the host Ni in the number of $3d$ electrons and produces a large local magnetic disturbance in $\text{Ni}_{1-x}\text{V}_x$ [25] by effectively reducing the Ni moments in its neighborhood. This suppression leads to the rapid average moment reduction [26] with increasing x , up to a small x_c , and to an inhomogeneous magnetization density in $\text{Ni}_{1-x}\text{V}_x$ as illustrated in Fig. 1(b). The locations of V are expected to mark the nonmagnetic defects that determine the distribution of the remaining *magnetic* Ni responsible for the magnetism. These magnetic Ni without any V neighbors contribute to long-range magnetic ordered regions or to the short-range magnetic clusters, which lead to the distinct signatures of a disordered QPT [12,15].

Ni rich $\text{Ni}_{1-x}\text{V}_x$ is expected to crystallize in a simple closed packed cubic fcc structure as does Ni, below $T_0(\text{Ni}) \approx 1400^\circ\text{C}$. Up to $x = 0.15$ no specific chemically ordered structure should form; under the ideal growth condition the elements V and Ni are thought to occupy the fcc lattice sites randomly [24]. While it is common for Ni rich binary alloys to display a random fcc lattice at high temperatures, an extended perfect solid solution phase down to low temperature is extremely rare and would make Ni-V a remarkable example. In most alloys the critical concentration x_c to suppress magnetic order is much higher than in the V alloy. Structural deviations develop more likely at higher x and towards low temperatures that modify strongly the magnetic behavior and magnetic cluster formation. For example, Ni-Pt exhibits a chemically ordered phase [27] below T_0 or short-range order correlations [9] if annealed at high temperatures $T_A > T_0$ at the critical concentration of $x_c \approx 0.5$. No chemically ordered phase is detected in Ni-Cu at $x_c \approx 0.5$, but preference for chemical clustering [28] is found above a miscibility temperature T_{misc} , indicating phase separation at lower temperatures. In both compounds with these different short-range correlations, the onset of magnetism (at x_c) depends critically on the chemical structure as the Ni environment changes with sample preparation [17,27].

No sign of phase separation or any miscibility temperature T_{misc} have been reported for Ni-V. An ordered structure, Ni_3V ,

is found at higher concentrations below $T_0 = 1050^\circ\text{C}$ [24]. At $x = 0.11$ a possible Ni_8V structure is indicated in the phase diagram. It only forms if V is substituted with larger elements [29], Ta or Nb, below $T_0 \approx 400^\circ\text{C}$. It is therefore not expected here as an ordered phase, but short-range order (SRO) is possible [30]. The SRO of selected concentrations $x = 1/9, 1/4, 1/3$ in Ni-V has been studied [30,31] around T_0 . The effective pair interaction (EPI) energies were found to be x dependent. While no clustering tendencies of closest neighbors of the same element were noted, ordering tendencies were recognized but get weaker [30] toward smaller x . Before testing for short-range signatures of these alternative structures or potential clustering, we model our data with the pair distribution function (PDF) of the random occupied fcc lattice.

IV. PAIR DISTRIBUTION FUNCTION ANALYSIS OF $\text{Ni}_{1-x}\text{V}_x$

The pair distribution function (PDF) [4] is essentially the Fourier transform of the total scattering function back into real space to probe for spatial correlations. We assume an ideal isotropic environment (expected in a powder) by averaging over all directions and consider only the modulus of wave vector transfer Q and distance r . $G(r) = 4\pi r[\rho - \rho_0]$ is a typical form of the PDF used for the PDFGUI [19] software; it gives the contrast between the pair density function ρ from the large distance average ρ_0 :

$$G(r) = 2/\pi \int_{Q_{\min}}^{Q_{\max}} [S(Q) - 1] Q \sin(Qr) dQ. \quad (1)$$

$S(Q)$ is the normalized total scattering function that includes the Bragg peaks and the diffuse scattering collected at the instrument (after background subtraction and calibration).

The typical PDF $G(r)$ of Ni-V is shown in Fig. 2. The blue open circles mark the $G(r)$ pellet data of $\text{Ni}_{0.85}\text{V}_{0.15}$ taken at low temperatures. All our Ni-V samples with different V concentration x , including Ni, produce similar $G(r)$ data that look like the pure Ni powder data [22]. The Ni-V data are described well using the PDFGUI software [19] employing a single phase fcc lattice with a partial Ni occupation of $(1-x)$ and V occupation of x according to the chemical composition of the sample, called *random* fit. The $G(r)$ of $\text{Ni}_{0.85}\text{V}_{0.15}$ does not present additional peaks besides the fcc lattice to indicate any secondary phase. The same is true for all $\text{Ni}_{1-x}\text{V}_x$ samples from $x = 0$ to $x = 0.15$ (not shown). This fit within the range of $1.75 \text{ \AA} < r < 20 \text{ \AA}$ is presented by the orange solid line. It yields a weighted residual factor Rw of 11%. The difference Δ of data and fit is shown underneath shifted by 14 units. This quick analysis already confirms that the samples do not deviate much from an fcc lattice with random occupation.

The direct scattering response $S(Q)$ of the Ni-V alloy does not reveal anything unusual as shown in Appendix A. $S(Q)$ just shows the expected fcc phase and no indication of superstructures and phase separation. Even the peak width in $S(Q)$ does not change with x in the alloy Ni-V. With PDFGUI [19] we extract the essential structural parameters from PDF, the cubic lattice constant a , and the atomic displacement parameter (ADP) u . The advantage is that these data can be collected at different ranges to distinguish local and global

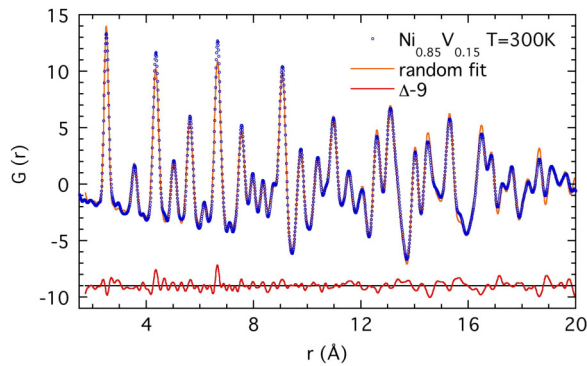


FIG. 3. PDF of $\text{Ni}_{0.85}\text{V}_{0.15}$ powder data (blue circles) taken at 300 K at NOMAD with random fit (orange line). The difference, $\Delta = \text{data} - \text{fit}$, is shown as a red line shifted by 9 units with residual $Rw = 11.5\%$.

environments. The ADP is the mean square atomic displacement from equilibrium position of one element averaged over time and sites. Since by far the strongest signal comes from Ni we consider only one isotropic parameter $u = u_{\text{Ni}}$ for Ni and chose the same value $u_{\text{V}} = u_{\text{Ni}} = u$ for V. The parameter u is extracted from the observed peak width in $G(r)$ that also includes effective correlation parameters and instrumental resolution parameters as explained in Appendix B.

On closer look the fit quality is not excellent and can be optimized by varying additional parameters in PDFGUI as explained more in detail in Appendix B. Mostly we were concerned about our sample setup—filling pellets in a wide can that does not meet the ideal homogeneous powder condition. Otherwise, we expect imperfection already in the pure Ni samples since all Ni-V pellets were fast cooled after annealing for optimal chemical distribution leading to some strain. In polycrystalline samples we also expect texture with different grain sizes and boundaries. To see what impact the inhomogeneous sample distribution of pellets has on the PDF data, we performed a proper *powder* experiment. The *powder* sample was produced from filing down some pellets. Figure 3 shows the PDF $G(r)$ for the same concentration $x = 0.15$ on a powder measured at NOMAD at 300 K. The different instrument and higher temperatures change some parameters—the peaks are broader and the lattice constant is larger—but the fcc lattice with random occupation also describes these powder data well. Again, little deviations of the fit are noticed. The fit improves with varying additional parameters (see Appendix B) indicating sample imperfections. The similar powder data confirm that the pellet data produce valuable results.

We collected structural data for longer ranges with $r_{\text{max}} = 20 \text{ \AA}$ for all $\text{Ni}_{1-x}\text{V}_x$ samples. The main lattice constant a is independent of the fit condition, while the ADP changes with r_{max} and with an optimized fit to account for lattice imperfections. To avoid disentangling various sample and setup effects in these samples we can focus on the most important local range that is still large enough to see the lattice with a range of $2a$. We analyze most structural data for short ranges with $r_{\text{max}} \approx 7 \text{ \AA}$. This small range offers the best quality fit, but is large enough to capture representative atom-atom spacing from the dominant Ni-Ni response. It is ideal to test the different alternative models beside the random model since

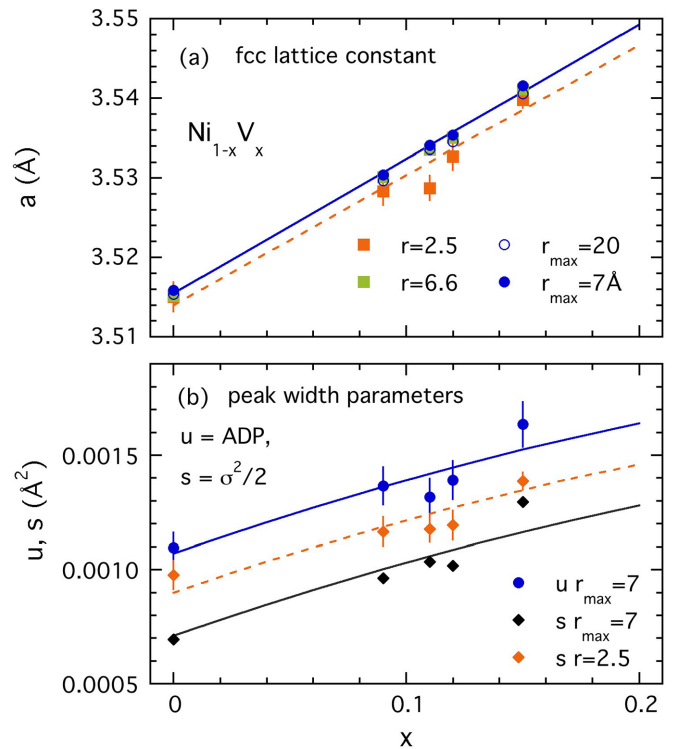


FIG. 4. (a) Lattice constant a , (b) atomic displacement parameter u , and half the nearest neighbor distance variance, $s = \frac{1}{2}\sigma^2$, vs V concentration x as refined from random fit for $\text{Ni}_{1-x}\text{V}_x$ at $T = 15 \text{ K}$. Solid (open) circles and black diamonds show data for $r_{\text{max}} = 7 \text{ \AA}$ (20 \AA). The squares and orange diamonds indicate data derived from individual peaks at a given distance r in \AA . The solid line in (a) is a fit of Eq. (2) with $a_0 = 3.5155 \text{ \AA}$ and $b = 0.048$. The data for the first peak follow the dashed line with a reduced $a_0 = 3.514 \text{ \AA}$ and $b = 0.047$. The solid lines in (b) follow Eq. (3) with the same a_0 , b and the fit constant $u_0 = 0.00107 \text{ \AA}^2$ and $s_0 = 0.00071 \text{ \AA}^2$. The dashed line starts at 0.0009 \AA^2 .

the range is below the superlattice size of the periodic phases employed in PDFGUI. The detailed parameters are available in Appendix B.

From $G(r)$ we evaluate the fcc lattice constant a and the ADP u and study their x dependence in $\text{Ni}_{1-x}\text{V}_x$. Figure 4 presents a and u of all samples at low $T = 15 \text{ K}$ as a function of the V concentration x evaluated mostly for $r_{\text{max}} = 7 \text{ \AA}$. For comparison some data are shown for longer ranges ($r_{\text{max}} = 20 \text{ \AA}$) and shorter ranges (first peak only). The increase of a with x is linear. It follows here simply Vegard's law [32]; the average atomic or ion radius increases with x due to (x) larger V atoms with atomic radius r_{V} and $(1-x)$ smaller Ni atoms with r_{Ni} :

$$a(x) = a_0(1 + bx) \quad \text{with } b = (r_{\text{V}} - r_{\text{Ni}})/r_{\text{Ni}}. \quad (2)$$

The line in Fig. 4(a) is a fit of Eq. (2) yielding $b = 0.048(1)$ and $a_0 = 3.5155(5) \text{ \AA}$. Such a linear lattice constant increase implies a constant atomic radius ratio of V and Ni (in the fcc lattice) of $r_{\text{V}}/r_{\text{Ni}} = 1 + b = 1.05$. This simple rigid sphere model is also supported by the pure metals. We find the same atomic ratio for V and Ni from the atomic distances at room temperature. The ratio of the nearest

neighbor distances of V (in bcc lattice) and of Ni is $d_V/d_{Ni} = \sqrt{3}/2 (3.04 \text{ \AA})/(3.54 \text{ \AA}) = 1.05$ (from [33]).

The peak width in $G(r)$ also changes with x . The extracted ADP u increases with x for $x \leq 0.15$ as shown in Fig. 4(b). This indicates further lattice defects that stem from the different V and Ni ion sizes and their interaction. We will test if a simple model of random diluted ions with different sizes is sufficient to explain such static lattice distortions. We collected data at low T , so that the ADP, $u = u_{\text{dyn}} + u_{\text{stat}}$, is most sensitive to static defects and just includes zero point motion; otherwise, the ADP is dominated by thermal motion at high T . The observed finite $u_0 = 0.0011 \text{ \AA}^2$ of Ni is close to the expected u_{dyn} estimate ($u = 0.0013 \text{ \AA}^2$) using the Debye model [34] for pure Ni (with low T Debye temperature $\Theta_D = 470 \text{ K}$ [35]). Since only minor variations of u_{dyn} with x are expected due to changes in Θ_D , the main increase of $u(x)$ is caused by u_{stat} . The parameter u is determined experimentally from the peak widths and the static changes can be estimated by the bond length variances.

In the simplest model of rigid spheres we predict the bond length variance σ_1^2 of a random occupied lattice with mean bond length ($\langle 2r \rangle \approx 2r_{\text{Ni}}$) of the first peak to change with x as $\sigma_1^2 = 2x(1-x)b^2r_{\text{Ni}}^2$. Here, we can find σ_1^2 or $s = \sigma_1^2/2$ by two different methods. We directly measure the first peak width σ_1 at $r_1 = a/\sqrt{2} \approx 2.5 \text{ \AA}$ assuming, e.g., a Gaussian form [36] as we discuss later. Or the bond length variance is determined by the fit parameters of PDFGUI in a larger range including many peaks up to r_{max} . The main parameter is the atomic displacement parameters u of both neighboring atoms corrected by correlation parameters [34] [see Eq. (B1) in Appendix B]. The ADP should show the same increase with x as half the bond length variance $s = \sigma^2/2$ or half the square of the peak width assuming the correlation parameters do not change much with x . Expressing the bond length $2r_{\text{Ni}}$ through the fcc lattice constant a_0 of Ni ($a_0/\sqrt{2} = 2r_{\text{Ni}}$) leads to a quantitative prediction for the change of $u(x)$ for random occupation:

$$u(x) = u_0 + \frac{1}{8}b^2a_0^2x(1-x). \quad (3)$$

The upper solid line in Fig. 4(b) shows the expected change of $u(x)$ using Eq. (3) with the already determined parameters, a_0 and b , from panel (a) and the fit parameter $u_0 = 0.00107 \text{ \AA}^2$. We see that the increase is well explained by static defects created only by the given size difference of the atoms with random occupation. Also, the determined half of the bond length variance of the closest Ni neighbor, $s = \frac{1}{2}\sigma^2$, follows the same fit simply shifted by 0.00035 \AA^2 [see lower solid line in Fig. 4(b)], confirming that the correlated motion does not change significantly with x . The uncertainty of variation in $u_{\text{dyn}}(x)$ stemming from the change of effective homogeneous lattice potential upon alloying is assumed to be about 6% [37] as indicated as error bars in the values of u .

In addition, we show the parameters from the first peak at location r_1 , namely the lattice constant $a_1 = \sqrt{2}r_1$ and width results of $s_1 = \sigma_1^2/2$, in Figs. 4(a) and 4(b), respectively. The first single peak data deviate somewhat from the other fit parameters derived from many peaks, while the spacing of further neighbors at $r = 6.6 \text{ \AA}$ agree well with higher ranges.

In this alloy the neutron response is dominated by Ni-Ni correlation and the V-Ni or V-V responses are nearly invisible. For close neighbors this specific responsive atom does not represent the average atom location as studied in more details in Ref. [36]. We note that the nearest Ni-Ni distance between actual Ni neighbors does change with x instead of the remaining constant. The observed average Ni-Ni distance is a bit smaller (by 0.05%) but seems nearly to adjust to the average atom-atom distance in the three dimensional alloy assessed by higher ranges. Otherwise, there are only very small variations of the lattice parameter with range. The average Ni-Ni distance increases with x and so do the variations. The first peak in Ni-V becomes clearly broader with x ; the half variance s_1 increases with x like $u(x)$. It follows Eq. (3) consistently with the observed $a(x)$ and a fit constant shown as a dashed line in Fig. 4(b). Maybe the increase is less, but higher precision data are needed for further details.

These estimates make the increase of peak width or u with x consistent with the expected lattice distortion of a random occupied lattice due to the mismatched atom sizes. Thus we do not see any additional dramatic change of lattice structures or local deformations evolving with x up to $x = 0.15$. We can summarize different strain assessments using PDF as follows. I. With a more ideal sample condition we should better discriminate set up effects from internal sample defects. Assuming now the worst sample quality, that the pure Ni sample has already some deviations from a main lattice spacing, we estimate a strain due to the presence of two simulated phases with different lattice constants $a_2 > a_1$, leading to a peak width increase with distance in $G(r)$. This yields a strain of $\epsilon_{2P} = 1/2(a_2 - a_1)/(a_2 + a_1)$ of order 0.35% that only slightly increases with x (by <10% for $x = 0.15$) as shown in Appendix B. II. Even if Ni might have already some crystalline imperfections, the major strain increase with x in Ni-V is due to mismatch of atomic sizes. The increase of the static defects that contribute to the ADP or peak width can give a strain estimate with $\epsilon_\sigma = \sigma_{\text{stat}}/r_{\text{atom}}$ [36], where $r_{\text{atom}} = a/2^{3/2}$ is the radius of the atom and $\sigma_{\text{stat}}^2 = \sigma^2 - \sigma_{\text{dyn}}^2$. If we assume that $x = 0$ is dominated by zero point motion σ_{dyn}^2 we estimate an increasing strain with x up to $\epsilon_\sigma = 0.032/1.3 = 2.5\%$ for $x = 0.15$. III. Another assessment of lattice strain from $G(r)$ is a change of lattice parameters with different range, fitting close range, or the first peak width yielding much larger spacing than the average parameters probed at large ranges. In Ni₂₀Pd₈₀ [38] values of $\epsilon_{\text{loc}} = (a_1 - a)/a = 0.4\%$ are found when the first peak location is compared with the average lattice spacing. The same effect is also noticed in HEAs such as NiCoCr and FeCoNiCrPd with $\epsilon_{\text{loc}} = 0.25\%$ [39] and $\epsilon_{\text{loc}} = 0.8\%$ [38], respectively. In Ni-V we do not see such large values in our neutron PDF study. The atomic size contrast might be smaller in this binary alloy, but the extreme different neutron cross sections of Ni and V do not allow for the assessment of the typical atom spacing for close distances [36]. Our change in lattice spacing in Ni-V evaluated with $r_{\text{max}} = 20 \text{ \AA}$ to $r_{\text{max}} = 7 \text{ \AA}$ gives a small positive value of $\epsilon_7 = a_7 - a_{20}/a_{20}$: already for Ni $\epsilon_7(x = 0) = 0.014\%$ and increases with x to $\epsilon_7(x = 0.15) = 0.028\%$. The apparent increase does not continue towards lower distances. The first peak location is smaller here not larger than the average

spacing. Closer distances such as the first peak only measure pure Ni-Ni distances that might be closer than the larger atom-atom distance. To probe proper atom-atom distances of direct neighbors an x-ray PDF study should be performed seeing both the V and the Ni atoms.

V. CLUSTERS AND ALTERNATE STRUCTURE MODELS

The PDF of our samples is well described by a fcc lattice with a random occupation, indicating a solid solution of V and Ni as ideally expected in this concentration range. Possible deviations are the formation of V clusters, an fcc lattice with locally enhanced vanadium concentration, which lead, in the extreme case, to segregation of large Ni-rich regions from V-rich regions. Another option is a chemical ordered structure with rather alternating Ni and V sites. We use here the local PDF to test these different Ni environments using the reduced PDF data of $\text{Ni}_{0.85}\text{V}_{0.15}$. We employ simple models in PDFGUI based on large periodic phases placing the two different atoms Ni and V at specific fcc lattice sites. The different response relies on the different cross section of the atoms, namely on the Ni occupation. Deviations from the original fcc lattice sites are not considered in the model; the static displacement was fitted using the random model through the ATP as discussed in the previous chapter. These simple models turn out to be effective to distinguish extreme atomic occupations. In a *random* fcc lattice up to a concentration of $x = 0.15$, V is expected to have only a few V neighbors out of the 12 nearest neighbors. The average V neighbor count is only $z_V = 12x = 1.8$ for $x = 0.15$. Most (90%) V have less than 4 V neighbors; 1 or 2 V neighbors are most likely. Evidence of V clusters larger than 4 V would signal a deviation from the ideal assumptions of a random occupation for $x = 0.15$. Since the neutron scattering length for Ni is dominant, the V-V and Ni-V correlations are less obvious in the neutron PDF; the Ni-Ni correlation is the major signal. We expect an average Ni neighbor count of a Ni site to be $z = 12(1 - x) = 10.2$ for the random occupied fcc lattice with $x = 0.15$. Larger V clusters than expected for random are recognized by larger Ni-rich regions with increased Ni-Ni coordination as directly observed in the first peak intensity in $G(r)$ as discussed below. To test for this, we probed different extreme models.

First, we check the response of a simulation of a *real* random structure for $\text{Ni}_{0.85}\text{V}_{0.15}$, a finite supercell phase with 5^3 cubic fcc unit cells where 500 Ni/V were placed once with the probability of 0.85/0.15. This *random cell* containing some small V clusters produces similar fit results to the previous *random model* that just used one unit cell with the same fractional occupation. The fit quality Rw is similar, as recorded in Table I.

To probe larger vanadium clusters we constructed a supercell phase in PDFGUI that contained large V clusters far away from each other: 38 V were placed in a spherical arrangement on an enlarged fcc lattice ($4 \times 4 \times 4$ cubic unit cells) with 256 atoms. This V38 model is illustrated in Fig. 5(a). The V clusters are $\sim 7 \text{ \AA}$ in size and are placed $\sim 14 \text{ \AA}$ from center to center, so that the distance in between (from edge to edge) is $\sim 7 \text{ \AA}$. This simple model of a V cluster with a single size reflects about the proper concentration of the sample. Analyzing the short-range correlation with restricted $r_{\text{max}} \approx 7 \text{ \AA}$ below

TABLE I. Fit quality of different models describing the local pair correlations in $\text{Ni}_{0.85}\text{V}_{0.15}$ for the two experimental data sets at 15 K and 300 K. The weighted residual factor Rw is listed for shorter fit range $r_{\text{max}} \sim 7 \text{ \AA}$ and longer range $r_{\text{max}} \sim 20 \text{ \AA}$. The concentration of the second phase (*) is about 15% determined with $r_{\text{max}} \approx 7 \text{ \AA}$ (see text for details).

r_{max}	15 K		300 K	
	6.9 \AA	20 \AA	7.1 \AA	20 \AA
Model	$Rw(\%)$	$Rw(\%)$	$Rw(\%)$	$Rw(\%)$
fcc random	7.87	11.5	6.93	11.5
Random cell 5a	7.92		7.01	
V4 cluster	8.77		7.94	
V13 cluster	8.55		7.72	
V38 cluster	8.87	(13.0)	8.22	(13.0)
Ni_8V	8.23	12.2	7.96	12.3
Ni_3V	10.2	22.2	12.3	22.2
Random+ Ni_8V^*	7.88	13	6.15	12
Random+ Ni_3V^*	7.35	10	5.93	10
Random+ Ni^*	7.74	12	6.70	11

the distance between the clusters allows for testing the effect of a V cluster without including the cluster-cluster correlation introduced in this periodic model. Figure 6 presents $G(r)$ of both models, the random fit and the V38 fit, with reduced $r_{\text{max}} = 6.9 \text{ \AA}$ using the 15 K NPDF data for $\text{Ni}_{0.85}\text{V}_{0.15}$. The V38 model does not create a dramatic change in peak intensity. However, a distinct change is noticed in the difference Δ between data and fit, in particular at the first peak in $G(r)$ at $\sim 2.5 \text{ \AA}$. This nearest neighbor peak intensity is sensitive to the average Ni-Ni coordination z . Δ of V38 presented in Fig. 6 by the green line (shifted by 9 units) shows more deviations than Δ of the random model shown as the red line above (shifted by 6 units). The V-cluster model with higher Ni-Ni first neighbor coordination z than the random model does not improve the fit. The better fit with reduced Rw value and lower z remains the random fit compared to the V38-cluster fit [see in Fig. 5(b) and Table I]. The refined parameters for the

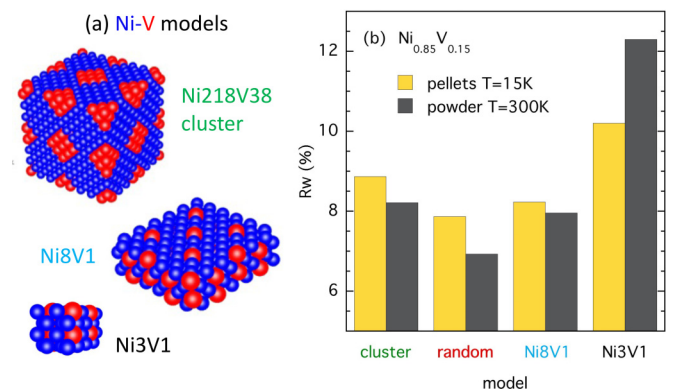


FIG. 5. (a) View of different alternate models of Ni-V with red V atoms and blue Ni atoms: V38 cluster model and structures are displayed with $2 \times 2 \times 2$ unit cells. (b) Fit quality of different models for pellet and powder data shows the random model with lowest residual factor Rw .

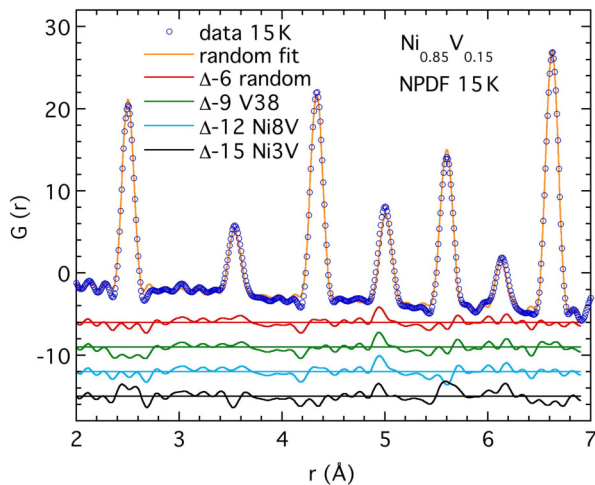


FIG. 6. Comparison of different models of local pair distribution, $\text{Ni}_{0.85}\text{V}_{0.15}$ data (taken at 15 K at NPDF), and difference ($\Delta = \text{data} - \text{model}$); models are fcc lattice with random occupation, V clusters, and Ni_8V and Ni_3V structure.

random distribution are listed in Appendix B in Table III and any deviations for other models are found in Appendix C.

For the study of smaller V clusters we had to make compromises of reduced concentration and reduced edge to edge distance. We prepared V4 clusters by defining 4 V within 32 atoms in a $2 \times 2 \times 2$ fcc supercell. The V concentration of the model ($x = 0.125$) is a bit lower than the sample concentration $x = 0.15$. With a cluster size of ~ 2.5 Å and a closest distance between the centers of ~ 7 Å, the edge to edge distance is rather short at ~ 5 Å, but still allows for probing mainly a single cluster correlation with r_{max} of ~ 7 Å. Also, a V13 cluster was prepared by defining 13 V within 108 atoms in a $3 \times 3 \times 3$ supercell. The V concentration of this model is $x = 0.12$. With a cluster size of ~ 5 Å and a distance between centers of ~ 11 Å, the edge to edge distance is ~ 6 Å. These smaller V-cluster models produce a similar PDF as the V38-cluster model with the same characteristic large first peak (not shown). The Rw factors are all higher than the value of the random model (see Table I).

The same V-cluster models were applied to the powder data of $\text{Ni}_{0.85}\text{V}_{0.15}$ collected at NOMAD at 300 K. Figure 7 displays the PDF fit results for the random and the V38-cluster model together with the data, in the same order as Fig. 6 presents the 15 K data. The residuals Rw of the different V-cluster fits as shown in Table I are all consistently larger than the Rw of the random fit. Table IV in Appendix B lists the refined parameters with the instrumental parameters for the random model. Most parameters remain similar for the other V-cluster models; Appendix C comments on some minor deviations. Although the fit quality of these different models does not change much, the local PDF provides a clear distinction between the models. The intensity of the first peak matches well the Ni-Ni coordination of an fcc lattice with random occupation and clearly deviates from the increased (Ni-Ni) neighbor count of the V-cluster models. It does not provide any evidence for large V clusters in Ni-V.

Other deviations from the random occupied fcc lattice are chemical ordered superstructures in a binary alloy. We are

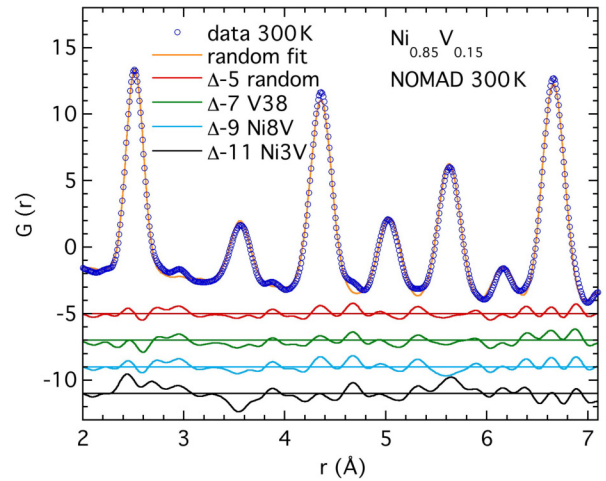


FIG. 7. Comparison of the same models of local pair distribution as in Fig. 6. The data are $\text{Ni}_{0.85}\text{V}_{0.15}$ powder data taken at 300 K at NOMAD.

probing here short-range and long-range order of Ni_8V and Ni_3V [see models in Fig. 5(a)]. The first potential chemical ordered structure in the Ni-rich region is Ni_8V . Ni_8Nb and Ni_8Ta order in this “ Ni_8Nb ” structure since the radius ratio is sufficiently large [29] ($r_{\text{Nb}}/r_{\text{Ni}} \approx r_{\text{Ta}}/r_{\text{Ni}} \approx 1.14$). The Ni_8Nb structure is a body-centered tetragonal structure (space group $I4/mmm$) with $9/2$ fcc unit cells with $a = b = \sqrt{9/2}c$. The Nb/V site has no similar neighbors; Ni has 1 or 2 Nb/V neighbors; the average Ni-Ni first neighbor count is $z = 10.5$. Although this ordered Ni_8V structure does not form as a long-range ordered phase at $x = 0.111$ short-range correlation can still be relevant in $\text{Ni}_{1-x}\text{V}_x$ in a wider concentration range [30]. The Ni_8V structure was prepared (as a $3 \times 3 \times 1$ fcc supercell with V at the origin and face center) to model the PDF data of $\text{Ni}_{0.85}\text{V}_{0.15}$ for short distances with $r_{\text{max}} \approx 7$ Å with PDFGUI under the same condition as the random fit. See model in Fig. 5(a). The difference Δ of data-model is displayed in Fig. 6 and Fig. 7 as a third line (in blue) shifted down by some units. The residual Rw , recorded in Table I, is small, but still larger than the random value. The difference between $z = 10.2$ and 10.5 , the effective average Ni-Ni neighbor count, is not very large, so farther neighbor correlations become relevant for the formation of the ordered structure.

The other superstructure Ni_3V forms from the disordered fcc phase below $T_0 = 1045^\circ\text{C}$ in a higher concentration range around $x = 0.25$, depending on sample growth conditions and heat treatments [24,29]. Ni_3V crystallizes in the SO_{22} structure, a body-centered tetragonal structure with 2 fcc unit cells along the c direction [40], where $c/a > 2$. V has only Ni neighbors and Ni has 2–4 V neighbors. The Ni-Ni coordination z is only 8–10. The short-range correlation of this Ni_3V structure was tested (using $1 \times 1 \times 2$ fcc supercell with V at origin and body center) as shown in Fig. 5. The difference Δ of data and model is presented as the lowest (black) line in Fig. 6 and Fig. 7. It shows obvious deviations, e.g., at the first peak in $G(r)$, and leads to the largest residual Rw as listed in Table I. This organized structure reduces the average Ni-Ni correlation to $z = 9.3$ which contradicts the experimental data. The refined parameters (see more in Appendix C) are

similar to the random results; only the lattice constants differ with $c/a = 2.006$.

We presented a detailed analysis of the most V rich sample $\text{Ni}_{0.85}\text{V}_{0.15}$, which would be expected to be the most prone to V clustering. Figure 5(b) summarizes the Rw for the main models clearly identifying the random model as the best description with the lowest Rw . Applying the same analysis on the other Ni-V samples with $x < 0.15$ gives similar results. The random model remains the best description for all. For all x , the residual factor Rw increases consistently by ~ 0.5 – 1% modeling the local PDF with the V-cluster model compared to the random model. The $x = 0.110$ pellet sample is described equally well with the Ni_8V structure or with the random model. These samples were annealed at high T for random distribution. To what extent short-range order of the Ni_8V remains in these samples cannot be resolved because of insufficient statistics. These data already demonstrate that no obvious V clustering and no large-scale phase separation occurs in Ni-V.

VI. TWO-PHASE MODELS

Besides testing alternate models such as random or superstructure, these two models and their contribution can be probed simultaneously for the same data set in a two-phase (2P) model. This is a simple way to notice deviations from a random occupied fcc lattice in regions within the sample and recognize atomic short-range correlations. Modeling the PDF of the $\text{Ni}_{0.85}\text{V}_{0.15}$ data with the random phase and the ordered phase Ni_3V (with a contribution of about $15\% \pm 8\%$) leads to a better description with a reduced Rw than the pure random model if the fit regime is restricted to $r_{\text{max}} \approx 7 \text{ \AA}$. Expanding the fit regime to $r_{\text{max}} = 20 \text{ \AA}$ does not improve Rw compared to the pure random model, signaling that only short-range correlations of Ni_3V are present. The refined lattice parameters are consistent with the expected values (see Appendix C). When the ordered phase is replaced by a second random phase (with independent lattice constant and contribution) the fit quality declines. This confirms that already weak short-range correlation of the Ni_3V structure is present in $\text{Ni}_{0.85}\text{V}_{0.15}$. We also tested for short-range correlation of Ni_8V with a 2P model. The best fit yields a Ni_8V phase contribution of about $14\% \pm 7\%$ with reasonable lattice parameters (see Appendix C). The residual does not show much improvement; the Ni_8V local environment is not very distinct from the random Ni environment. More distinct longer-range correlations different from random are not confirmed as expected for our samples annealed at high temperatures.

A 2P model can also be used to probe phase separation of Ni and V or large concentration gradients in Ni-V by separating pure Ni regions from diluted Ni-V regions. Phase separation of Ni+Ni-X has been suggested for Ni-Rh [41] forming below a miscibility temperature from a disordered fcc phase at higher temperatures. Modeling the PDF data with a pure Ni phase (with constrained Ni parameters) and a random occupied $\text{Ni}_{1-x}\text{V}_x$ phase ($x \geq 0.15$) with adjustable parameters yields a slightly better fit than the single-phase random model if the fit range is restricted to a short range of $r_{\text{max}} \approx 7 \text{ \AA}$. Table I shows the Rw factors. The indicated contribution of the Ni phase is $12\% \pm 5\%$. Probing for a

Ni-rich region up to $r_{\text{max}} = 20 \text{ \AA}$ returns only zero or a negative contribution. If 12% of the pure Ni phase is imposed, the Rw factor increases. Therefore, large Ni regions beyond the random statistics can be excluded. Pure Ni regions become more likely within a smaller volume of radius r_{max} . The observed value of $\sim 12\%$ is still higher than the probability of a pure $x = 0$ region within $r_{\text{max}} = 7 \text{ \AA}$ ($< 1\%$) but matches the probability of $x = 0$ below 3 \AA (of 12% of Ni with only Ni neighbors) in a randomly diluted NiV sample with $x = 0.15$. Some small size Ni-rich regions are noticed in $x = 0.15$ that point to minor local deviations from the average concentration and the ideal crystal structure. It was shown that, in Ni-Cr nanoparticles [42] with a diameter of $d < 10 \text{ nm}$, different chemical environments were found at the surface compared to the bulk due to Cr segregation to the surface. We expect here much larger crystallites in our polycrystalline samples, but different Ni environment at grain boundaries are certainly possible. Grain boundary-aided nucleation of growth of the ordered Ni_3V structure was investigated in a melt spun $\text{Ni}_{0.75}\text{V}_{0.25}$ alloy [43]. With simple models these PDF results support that, in Ni-V, minor local concentration gradients are present but there is no phase separation on larger scales. Further studies employing advanced models [44] on PDF data collected on better powder samples are promising to reveal more details.

VII. CONCLUSION

We present a detailed pair distribution (PDF) analysis from neutron scattering data of the $\text{Ni}_{1-x}\text{V}_x$ alloy. This study answers the main question by confirming that our Ni-V samples meet all criteria for a solid solution at low temperatures that are relevant for the magnetism. Although the sample setup is not ideal and only simple models are tested random occupation is distinct from ordered and extreme clustered local environments in PDF. The results demonstrate that the local PDF is a powerful method to probe the relevant Ni environment in the $\text{Ni}_{1-x}\text{V}_x$ samples to reveal many details. The fcc lattice is the best model when V and Ni are occupying the fcc lattice sites at random. V-cluster models are worse descriptions. The results exclude distinct phase segregation of V and Ni-rich regions. Other chemically ordered structure models show deviations from the data due to the different local environment. The PDF analysis reveals at most weak short-range correlations of Ni_3V in $\text{Ni}_{0.85}\text{V}_{0.15}$. Also, the increase of the lattice constant and the atomic displacement parameters (ADP) with x is consistent with the simple packing of solid spheres (of V and Ni atoms) in a fcc lattice with occupational disorder. The atomic size mismatch explains the increased strain in the alloy. This simple PDF analysis concludes that $\text{Ni}_{1-x}\text{V}_x$ is a system with potential short-range order at specific concentrations, but not prone to chemical clustering like Ni-Cu. $\text{Ni}_{1-x}\text{V}_x$ shows more preference for ordering than for clustering. V clustering as a cause for magnetic cluster formation can be excluded. The chemical ordering correlations are rather weak for $x \leq 0.15$. The local Ni environment in Ni_8V is not very distinct from the random occupation. That makes $\text{Ni}_{1-x}\text{V}_x$ a remarkable system that favors random occupation when prepared with high annealing temperatures and cooled down rapidly.

How much any weak remnants of chemical ordering impact the magnetism here could be studied further with optimized samples and more advanced models. Since the actual V location and potential V clusters are of high interest for a complete structural determination and also relevant as a source of magnetic clusters, a complementary x-ray PDF study becomes essential as a next step. General x rays provide a more similar cross section of the elements Ni/V with atomic number ratio of $(29/23)^2 = 1.5$. Successful x-ray PDF data from synchrotron sources [45] and improved analysis methods with optimized models using RMC [44] offer advanced tools for better precision analysis. Possible small V clusters and the extent of short-range order (SRO) in Ni-V can be refined as a function of V concentration. This requires proper sample preparation in acceptable isotropic *powder* form. After these promising PDF results on different sample setups we do not expect the essential sample quality to change after the filing process, but all sample preparation and treatment protocols manipulate easily sample imperfection in these alloys.

We expect the possible SRO to be dependent on V concentration and on sample preparation. Regions with SRO might not lead to the formation of Ni-rich regions but could still modify the magnetic cluster distribution. Deviations from *perfect random* are most likely to occur close to $x \approx 0.11$, the concentration of the ordered phase that is close to the critical concentration $x_c = 0.116$, where the ferromagnetic order breaks down with most dominant *magnetic* clusters. The best test sample would be Ni-V with $x = 0.110$ or better of $x = 0.111$ using samples prepared with different annealing temperatures T_A provoking different SRO. PDF measurements on powdered samples test for the structural SRO, while the impact on magnetic clusters gets revealed through comparison with magnetic measurements. To directly observe the *magnetic* clusters in these polycrystals (magnetic) mPDF methods [46,47] remain too challenging in this small moment system but direct neutron scattering measurements like SANS seem feasible to characterize magnetic correlation at $x \approx 0.11$ [16,48].

ACKNOWLEDGMENTS

This work has benefited from the use of the NPDF instrument at the Los Alamos Neutron Science Center, Los Alamos National Laboratory, funded by the US Department of Energy. Part of this research was conducted at the NOMAD instrument at the Spallation Neutron Source, a US Department of Energy Office of Science User Facility operated by Oak Ridge National Laboratory.

APPENDIX A: SCATTERING DATA

We derive the PDF from wide angle normalized scattering data $S(Q)$ and analyze $G(r)$ taking advantage of the spatial variations at different ranges to detect defects. The direct $S(Q)$ data of Ni-V do not reveal obvious imperfections. Figure 8 gives an overview of the Ni-V alloy with $x = 0.15$ compared to pure Ni. We do not expect a new structure different than a fcc structure. $S(Q)$ does not show any phase separation or minority phase. No long-range ordered phase of Ni_3V is present, which is the most stable phase beside

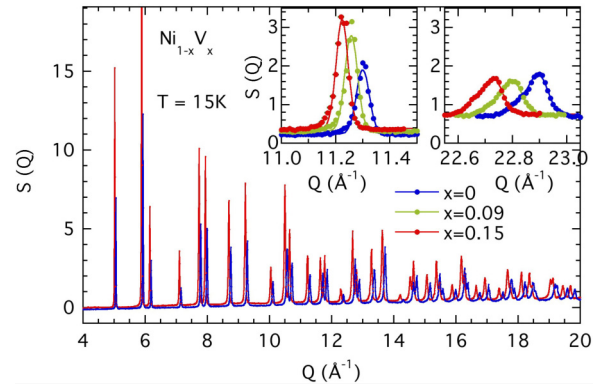


FIG. 8. Example of direct scattering data $S(Q)$ as function of wave vector Q of Ni-V for $x = 0.15$ and $x = 0$. The insets show individual peaks for selected x at a lower and higher Q value.

the Ni fcc phase. The Bragg peaks are shifted as the lattice constant increases with x . The inset contrasts the $(6,2,0)$ peak at low $Q \approx 11 \text{ \AA}^{-1}$ and a double peak $(10,8,0)+(7,7,1)$ at higher $Q \approx 23 \text{ \AA}^{-1}$ for several V concentrations x . They keep their width upon alloying with x , while the intensity ratio (low/high Q) changes. The intensity of the peaks decays faster towards Q with higher x . So we expect the complementary behavior in PDF, an increasing peak width in $G(r)$ with x in Ni-V, as we discuss in the main text.

APPENDIX B: PDF PARAMETERS OF RANDOM MODEL

This section lists the detailed fit parameters from the PDF analysis including the control parameters. We used the PDFGUI program [19] to analyze the data. Besides the crystal lattice and atomic position parameters it also determines their variations, the atomic displacement parameters ADP, and contains two simple control parameters to accommodate the resolution of the instrument configuration. The ADP parameter u is extracted from the observed peak width in $G(r)$. u is essentially the isotropic ADP of Ni. We set formally the same parameter for V; even if the real $u(\text{V})$ might be a bit larger than $u(\text{Ni})$ it does not change the fit since the V response is nearly invisible. The effective parameters δ_2 and δ_1 are introduced to correct the uncorrelated width for a correlated motion of close pairs [34]. The square of the peak width (HWHM), the experimental variance of the mean bond length σ^2 , is then produced by these simple fit parameters in the PDFGUI program:

$$\sigma^2 = 2u[1 - \delta_2/r^2 - \delta_1(T)/r + (r Q_{\text{broad}})^2]. \quad (\text{B1})$$

Q_{broad} and Q_{damp} are the instrumental control parameters that model the instrumental peak width increase with distance r and effective intensity decay of $G(r)$ in PDFGUI. The values of both parameters are determined by a calibration standard (typically a Si powder). For low temperatures (15 K) $\delta_1 = 0$; for high temperature (300 K) δ_1 dominates so that we kept $\delta_2 = 0$.

Table II shows the fit parameters for $x = 0.15$ and $x = 0$ for a larger range of $r_{\text{max}} = 20 \text{ \AA}$. The fit quality of the random fcc lattice with the default calibrated instrumental parameter setting (called Q_0) is satisfactory, yielding a residual $Rw = 11\%$ for $x = 0.15$. Surprisingly, the fit quality of $x = 0$ is

TABLE II. Refined fit parameters of $\text{Ni}_{1-x}\text{V}_x$ at 15 K of the fcc random model: fcc lattice constant a , (isotropic) atomic displacement parameter u , correlated motion parameters δ_2 , δ_1 , overall *scale* factor, and weighted residual factor Rw within fit range $r_{\text{max}} = 20 \text{ \AA}$. Q_L indicates optimized fit using enhanced resolution parameters ($Q_{\text{damp}} = 0.02 \text{ \AA}^{-1}$ and $Q_{\text{broad}} = 0.035 \text{ \AA}^{-1}$).

$\text{Ni}_{1-x}\text{V}_x$	$x = 0$	$x = 0$ QL	$x = 0.15$	$x = 0.15$ QL
a (\AA)	3.51538(1)	3.51540(1)	3.54056(1)	3.54058(1)
u (\AA^2)	0.001456(3)	0.001132(2)	0.002050(3)	0.001610(3)
δ_2 (\AA^2)	3.63(3)	2.32(4)	2.84(2)	1.26(3)
<i>Scale</i>	0.4584(6)	0.4669(6)	0.6355(7)	0.6473(7)
Rw (%)	18.8	17.2	11.0	7.94

even worse. We varied the lower limit $Q_{\text{min}} > 0.1 \text{ \AA}^{-1}$ to get the $G(r)$ from $S(Q)$ and found that a higher $Q_{\text{min}} = 0.18 \text{ \AA}^{-1}$ produced the best PDF with lowest Rw and least underlying wiggles. Since the setup is not optimal for these pellet samples it is not clear if the very low Q signal in $S(Q)$ stems from the sample or environment. The powder sample at high temperatures did not show any such problem. If we modify the resolution parameters by taking the pure Ni as calibration sample we find larger values called Q_L , which optimize the fit quality for all. The Q_0 values for NPDF are $Q_{\text{damp}} = 0.006 \text{ \AA}^{-1}$ and $Q_{\text{broad}} = 0.002 \text{ \AA}^{-1}$; the Q_L values become $Q_{\text{damp}} = 0.02 \text{ \AA}^{-1}$ and $Q_{\text{broad}} = 0.035 \text{ \AA}^{-1}$. With these larger Q_L values the fit quality improves to lower Rw values as seen in Table II. This implies that the peak widths grow larger and the PDF intensity decays faster with r than ideally expected for a perfect lattice. Modifying the resolution parameters is used here as a diagnostic tool to notice sample imperfections. It demonstrates that already lattice imperfections are present in pure Ni grown by the same protocol as the other alloys. More details of modeling resolution effects and their impact on data analysis can be found in [49]. Note that especially the largest Rw is observed for $x = 0$, which seems less likely to relate to the internal sample quality but to the sample arrangement. Our pure Ni samples contained pellets with the largest size of ~ 4 mm that lead to the most inhomogeneous distribution within the sample can. We suspect that the sample density variation of several pellets instead of the ideal isotropic powder is responsible for additional wiggles in the PDF data that causes the high Rw .

A reduced range offers the best description independent of resolution effects. Table III presents the structural parameters

TABLE III. Refined fit parameters of $\text{Ni}_{1-x}\text{V}_x$ at 15 K of the fcc random model: fcc lattice constant a , (isotropic) atomic displacement parameter u , correlated motion parameters δ_2 , δ_1 , overall *scale* factor, and weighted residual factor Rw within fit range $r_{\text{max}} = 6.9 \text{ \AA}$.

$\text{Ni}_{1-x}\text{V}_x$	$x = 0$	$x = 0.09$	$x = 0.15$
a (\AA)	3.51589(7)	3.53043(8)	3.54158(6)
u (\AA^2)	0.001095(7)	0.001365(9)	0.001635(8)
δ_2 (\AA^2)	2.18(4)	1.84(6)	1.30(4)
<i>Scale</i>	0.452(1)	0.540(1)	0.640(1)
Rw (%)	17.7	14.1	7.87

TABLE IV. Refined fit parameters of $\text{Ni}_{0.85}\text{V}_{0.15}$ at 300 K of the fcc random model. Note the similar fit quality (Rw) and parameters for different settings: for $r_{\text{max}} \approx 7 \text{ \AA}$ with Q_0 and for $r_{\text{max}} = 20 \text{ \AA}$ with Q_L . Q_L indicates optimized fit using enhanced resolution parameters ($Q_{\text{damp}} = 0.033 \text{ \AA}^{-1}$ and $Q_{\text{broad}} = 0.040 \text{ \AA}^{-1}$).

r_{max} (\AA)	20	20 QL	7.1
a (\AA)	3.5608(3)	3.5608(3)	3.5615(8)
u (\AA^2)	0.0097(1)	0.0077(1)	0.0079(3)
δ_1 (\AA)	1.69(4)	1.37(5)	1.37(7)
<i>Scale</i>	0.675(7)	0.693(7)	0.69(1)
Rw (%)	11.5	8.45	6.93

for selected Ni-V with $r_{\text{max}} \approx 7 \text{ \AA}$. These values are shown for the default Q_0 resolution parameters, which are the same as for the Q_L setup for this short range. They also agree to the larger range results evaluated with Q_L . These test results show that the lattice constant a is independent of the fit condition (Q_0 or Q_L) for any range, but not the atomic displacement parameter ADP, called u . At the end the contrast of $u(x)$ to $u(x = 0)$ is about the same, so that the main analysis does not alter through effective control parameters. To keep the analysis most transparent with least parameters the short-range 7 \AA data with default resolution are chosen for the main investigation. The overall free scale factor does not change more than 2% for each concentration probing different control parameters.

For comparison, we performed another experiment on a powder sample produced from filing down some pellets for $x = 0.15$. Table IV lists the structural parameters for the similar shorter range of 7 \AA and the longer range of 20 \AA from a different instrument NOMAD. Again, the short-range data are independent of the resolution setting. For NOMAD Q_0 stands for $Q_{\text{damp}} = 0.018 \text{ \AA}^{-1}$, $Q_{\text{broad}} = 0.019 \text{ \AA}^{-1}$ and Q_L for $Q_{\text{damp}} = 0.033 \text{ \AA}^{-1}$, $Q_{\text{broad}} = 0.04 \text{ \AA}^{-1}$. But they change for $r_{\text{max}} = 20 \text{ \AA}$; the proper instrumental parameters with low Q_0 values produce a residual factor $Rw = 11.5\%$ that reduces to $Rw = 8.45\%$ with enhanced Q_L values.

The common *reduction* of Rw for all x by increasing the instrumental parameters from Q_0 to Q_L at different instruments relates most likely to the sample quality. Alternatively to enhancing the resolution parameters, these lattice imperfections can be modeled by simple tools in PDFGUI through extra parameters, keeping the calibrated values Q_0 . Through a two-phase (2P) model with two fcc lattices that only differ in lattice constants ($a_2 > a_1$) the strain $\Delta a/a$ can be estimated where $\Delta a = (a_2 - a_1)$ and $a = (a_2 + a_1)/2$. Also a nanoparticle diameter dia is available in PDFGUI to estimate a finite crystallite size. The best 2P model fit yields a lattice variation or effective strain $\Delta a/a$ of 0.353% for $x = 0$ that increases slightly to 0.378% for $x = 0.15$. These values are consistent with the alternate description using an increased $Q_{\text{broad}} = Q_L$ value expecting $\Delta a/a \approx 2\sqrt{u} Q_{\text{broad}}$. The increased $Q_{\text{damp}} = Q_L$ value corresponds to a finite crystallite size in the order of 100 \AA ($dia \approx 2/Q_{\text{damp}}$). Within the 2P model the fit quality improves only a bit for $x = 0.15$ from $Rw = 8.26\%$ to $Rw = 7.96\%$ with a finite $dia \approx 300 \text{ \AA}$, while for $x < 0.15$ Rw remains unchanged with insignificant high $dia > 300 \text{ \AA}$ values.

Both alternative models, two-phase (2P) with Q_0 or one phase with Q_L , yield essentially the same fit with similar parameters and fit qualities Rw evaluated at a range of 20 Å.

APPENDIX C: PDF PARAMETERS OF OTHER MODELS

Here we discuss the essential fit parameters for testing other models than random using single phase and two phases within PDFGUI. The PDF of Ni-V with $x = 0.15$ is fitted with the same control parameters for the short range of $r_{\min} = 1.75$ Å to $r_{\max} \approx 7$ Å for all models: from models with random occupation to cluster models with selected V-cluster sizes to superstructures (Ni3V, Ni8V). Table I shows the fit quality through the weighted residual factor Rw . The detailed fit parameters are not very different from the random model as listed in Tables III and IV. The scale factor varies less than 1% for nearly all models including the total scale for two phase models, except for the large cluster model V38 where it is reduced by 4%. For full information we comment on some deviating parameters of the other models. We call a_{15} , u_{15} , and δ_{15} the values for the random model. The cluster

models produce the same parameters except the correlation parameter is smaller, decreasing further with increasing the clusters' size to V38, where δ_1 becomes 1.17 and δ_2 reduces to $\delta_2 = 0.49$. Also the refined parameters of the Ni8V structure are similar to the random fit with $c = a_{15}$. The Ni3V structure allows for two different lattice constants with $a = 0.999a_{15}$ and $c/a = 2.006$. The ADP is somewhat larger with $u = 0.0021$ Å² (15 K) and $u = 0.0087$ Å² (300 K).

We probed two phase models to check for short-range order. The most obvious ordered phase is Ni3V. $G(r)$ of Ni_{0.85}V_{0.15} is fitted with $r_{\max} \approx 7$ Å using two phases—one with random occupation and one with the ordered phase Ni3V. The best fit yields a contribution of $15\% \pm 8\%$ of Ni3V with a reduced Rw as listed in Tables III and IV. The refined lattice parameters are $a_{\text{random}} = 1.001a_{15}$ and $a_{31} = 0.993a_{15}$ with $c_{31}/a_{31} = 2.03(1)$ for the random and the ordered Ni3V phase, respectively. Using Ni8V for the second ordered phase yields a similar contribution of $14\% \pm 7\%$ for the best fit but not a distinct improvement in Rw compared to the pure random model. The refined parameters are $a_{\text{random}} = 1.001a_{15}$ and $c_{81} = 0.998a_{15}$ for the random and the ordered Ni8V phase, respectively.

-
- [1] S. Kobayashi, K. Sato, E. Hayashi, T. Osaka, T. J. Konno, Y. Kaneno, and T. Takasugi, Alloying effects on the phase equilibria among Ni(A1), Ni₃Al(L12) and Ni₃V(D022) phases, *Intermetallics* **23**, 68 (2012).
- [2] B. Cantor, I. Chang, P. Knight, and A. Vincent, Microstructural development in equiatomic multicomponent alloys, *Mater. Sci. Eng. A* **375-377**, 213 (2004).
- [3] J.-W. Yeh, S.-K. Chen, S.-J. Lin, J.-Y. Gan, T.-S. Chin, T.-T. Shun, C.-H. Tsau, and S.-Y. Chang, Nanostructured high-entropy alloys with multiple principal elements: Novel alloy design concepts and outcomes, *Adv. Eng. Mater.* **6**, 299 (2004).
- [4] T. Egami and S. J. L. Billinge, *Underneath the Bragg Peaks: Structural Analysis of Complex Materials* (Pergamon Press, Elsevier, Oxford, England, 2003).
- [5] J. M. Cowley, An approximate theory of order in alloys, *Phys. Rev.* **77**, 669 (1950).
- [6] F. Bölling, Ferro- und paramagnetisches Verhalten in den Mischkristallen des Nickels mit Vanadium, Rhodium und Platin im Temperaturbereich von 14° bis 1000° K, *Phys. Kondens. Materie* **7**, 162 (1968).
- [7] A. Amamou and B. Loegel, Giant moment in nickel solid solutions, *J. Phys. F: Met. Phys.* **3**, L79 (1973).
- [8] V. Suresh Babu, A. S. Pavlovic, and M. S. Seehra, Rapid loss of magnetic order in Ni on alloying with Cr, Mo, Re, and Si, *J. Appl. Phys.* **79**, 5230 (1996).
- [9] J. A. Rodriguez, S. C. Moss, J. L. Robertson, J. R. D. Copley, D. A. Neumann, and J. Major, Neutron scattering studies of short-range order, atomic displacements, and effective pair interactions in a null-matrix ⁶²Ni_{0.52}Pt_{0.48} crystal, *Phys. Rev. B* **74**, 104115 (2006).
- [10] M. Brando, D. Belitz, F. M. Grosche, and T. R. Kirkpatrick, Metallic quantum ferromagnets, *Rev. Mod. Phys.* **88**, 025006 (2016).
- [11] M. Nicklas, M. Brando, G. Knebel, F. Mayr, W. Trinkl, and A. Loidl, Non-Fermi liquid behavior at a ferromagnetic quantum critical point in Ni_xPd_{1-x}, *Phys. Rev. Lett.* **82**, 4268 (1999).
- [12] T. Vojta, Rare region effects at classical, quantum, and non-equilibrium phase transitions, *J. Phys. A: Math. Gen.* **39**, R143 (2006).
- [13] S. Ubaid-Kassis, T. Vojta, and A. Schroeder, Quantum Griffiths phase in the weak itinerant ferromagnetic alloy Ni_{1-x}V_x, *Phys. Rev. Lett.* **104**, 066402 (2010).
- [14] R. Wang, A. Gebretsadik, S. Ubaid-Kassis, A. Schroeder, T. Vojta, P. J. Baker, F. L. Pratt, S. J. Blundell, T. Lancaster, I. Franke, J. S. Möller, and K. Page, Quantum Griffiths phase inside the ferromagnetic phase of Ni_{1-x}V_x, *Phys. Rev. Lett.* **118**, 267202 (2017).
- [15] T. Vojta, Quantum Griffiths effects and smeared phase transitions in metals: Theory and experiment, *J. Low Temp. Phys.* **161**, 299 (2010).
- [16] S. Bhattarai, H. Adawi, J.-G. Lussier, A. Gebretsadik, M. Dzero, K. L. Krycka, and A. Schroeder, Evolution of short-range magnetic correlations in ferromagnetic Ni-V alloys, *Phys. Rev. B* **107**, 054409 (2023).
- [17] C. Tranchita and H. Claus, Magnetism in Ni-Cu alloys, *Solid State Commun.* **27**, 583 (1978).
- [18] T. Proffen, V. Petkov, S. J. L. Billinge, and T. Vogt, Chemical short range order obtained from the atomic pair distribution function, *Z. Kristallogr. Cryst. Mater.* **217**, 47 (2002).
- [19] C. L. Farrow, P. Juhas, J. W. Liu, D. Bryndin, E. S. Bozin, J. Bloch, T. Proffen, and S. J. L. Billinge, PDFfit2 and PDFgui: Computer programs for studying nanostructure in crystals, *J. Phys.: Condens. Matter* **19**, 335219 (2007).
- [20] A. Schroeder, R. Wang, P. J. Baker, F. L. Pratt, S. J. Blundell, T. Lancaster, I. Franke, and J. S. Möller, Probing the magnetic phases in the Ni-V alloy close to the disordered ferromagnetic

- quantum critical point with μ SR, *J. Phys.: Conf. Ser.* **551**, 012003 (2014).
- [21] T. Proffen, T. Egami, S. Billinge, A. Cheetham, D. Louca, and J. Parise, Building a high resolution total scattering powder diffractometer—upgrade of NPD at MLNSC, *Appl. Phys. A* **74**, s163 (2002).
- [22] J. Neuefeind, M. Feygenson, J. Carruth, R. Hoffmann, and K. K. Chiple, The Nanoscale Ordered MAterials Diffractometer (NOMAD) at the Spallation Neutron Source (SNS), *Nucl. Instrum. Methods Phys. Res., B* **287**, 68 (2012).
- [23] P. F. Peterson, M. Gutmann, T. Proffen, and S. J. L. Billinge, *PDFgetN*: A user-friendly program to extract the total scattering structure factor and the pair distribution function from neutron powder diffraction data, *J. Appl. Crystallogr.* **33**, 1192 (2000).
- [24] J. F. Smith, O. N. Carlson, and P. G. Nash, The Ni-V (nickel-vanadium) system, *Bull. Alloy Phase Diagr.* **3**, 342 (1982).
- [25] M. F. Collins and G. G. Low, The magnetic moment distribution around transition element impurities in iron and nickel, *Proc. Phys. Soc.* **86**, 535 (1965).
- [26] J. Friedel, Metallic alloys, *Nuovo Cim.* **7**, 287 (1958).
- [27] C. E. Dahmani, M. C. Cadeville, J. M. Sanchez, and J. L. Morán-López, Ni-Pt phase diagram: Experiment and theory, *Phys. Rev. Lett.* **55**, 1208 (1985).
- [28] J. Vrijen and S. Radelaar, Clustering in Cu-Ni alloys: A diffuse neutron-scattering study, *Phys. Rev. B* **17**, 409 (1978).
- [29] H. A. Moreen, R. Taggart, and D. H. Polonis, Ni_8X phases in the systems Ni-V, Ni-V-Nb, and Ni-V-Ta, *J. Mater. Sci.* **6**, 1425 (1971).
- [30] D. Le Bolloc'h, A. Finel, and R. Caudron, Concentration dependence of the short-range order in the Ni-V and Pt-V systems, *Phys. Rev. B* **62**, 12082 (2000).
- [31] M. Barrachin, A. Finel, R. Caudron, A. Pasturel, and A. Francois, Order and disorder in Ni_3V : Effective pair interactions and the role of electronic excitations, *Phys. Rev. B* **50**, 12980 (1994).
- [32] L. Vegard, Die Konstitution der Mischkristalle und die Raumbfüllung der Atome, *Z. Phys.* **5**, 17 (1921).
- [33] A. W. Hull, The crystal structures of the common elements, *J. Franklin Inst.* **193**, 189 (1922).
- [34] I.-K. Jeong, R. H. Heffner, M. J. Graf, and S. J. L. Billinge, Lattice dynamics and correlated atomic motion from the atomic pair distribution function, *Phys. Rev. B* **67**, 104301 (2003).
- [35] M. Dixon, F. E. Hoare, and T. M. Holden, The low-temperature specific heats of some nickel-based iron and copper alloys, *Proc. R. Soc. London A* **303**, 339 (1968).
- [36] L. Owen, H. Stone, and H. Playford, The assessment of local lattice strains in alloys using total scattering, *Acta Mater.* **170**, 38 (2019).
- [37] The ratio of $\Theta_D(\text{V})/\Theta_D(\text{Ni}) = 380\text{K}/470\text{K}$ [35,50] or $\Theta_D(\text{Ni}_3\text{V})/\Theta_D(\text{Ni}) = 520\text{K}/470\text{K}$ [51] might cause a change of $u_{\text{Ni}} \sim 1/\Theta_D$ with $\Delta x = 0.15$ of 3% or 6%, if linearly interpolated. The variations in the low-temperature specific heat coefficient β in Ni-V [52] suggest a possible change in Θ_D of less than 8% for $x < 0.15$.
- [38] Y. Tong, S. Zhao, K. Jin, H. Bei, J. Ko, Y. Zhang, and F. Zhang, A comparison study of local lattice distortion in $\text{Ni}_{80}\text{Pd}_{20}$ binary alloy and FeCoNiCrPd high-entropy alloy, *Scr. Mater.* **156**, 14 (2018).
- [39] Y. Tong, K. Jin, H. Bei, J. Ko, D. Pagan, Y. Zhang, and F. Zhang, Local lattice distortion in NiCoCr, FeCoNiCr, and FeCoNiCrMn concentrated alloys investigated by synchrotron x-ray diffraction, *Mater. Des.* **155**, 1 (2018).
- [40] W. Lin, J. H. Xu, and A. J. Freeman, Electronic structure, cohesive properties, and phase stability of Ni_3V , Co_3V , and Fe_3V , *Phys. Rev. B* **45**, 10863 (1992).
- [41] J. Teeriniemi, J. Huisman, P. Taskinen, and K. Laasonen, First-principles modelling of solid Ni-Rh (nickel-rhodium) alloys, *J. Alloys Compd.* **652**, 371 (2015).
- [42] M. Bohra, P. Grammatikopoulos, R. E. Diaz, V. Singh, J. Zhao, J.-F. Bobo, A. Kuronen, F. Djurabekova, K. Nordlund, and M. Sowwan, Surface segregation in chromium-doped NiCr alloy nanoparticles and its effect on their magnetic behavior, *Chem. Mater.* **27**, 3216 (2015).
- [43] J. Singh, M. Sundararaman, S. Banerjee, and P. Mukhopadhyay, Evolution of order in melt-spun Ni-25at.%V alloys, *Acta Mater.* **53**, 1135 (2005).
- [44] L. Owen, H. Playford, H. Stone, and M. Tucker, A new approach to the analysis of short-range order in alloys using total scattering, *Acta Mater.* **115**, 155 (2016).
- [45] S. J. L. Billinge, The rise of the x-ray atomic pair distribution function method: A series of fortunate events, *Philos. Trans. R. Soc. A* **377**, 20180413 (2019).
- [46] B. A. Frandsen, X. Yang, and S. J. L. Billinge, Magnetic pair distribution function analysis of local magnetic correlations, *Acta Crystallogr. A* **70**, 3 (2014).
- [47] B. A. Frandsen, R. Baral, B. Winn, and V. O. Garlea, Magnetic pair distribution function data using polarized neutrons and *ad hoc* corrections, *J. Appl. Phys.* **132**, 223909 (2022).
- [48] A. Schroeder, S. Bhattarai, A. Gebretsadik, H. Adawi, J.-G. Lussier, and K. L. Krycka, Magnetic correlations in the disordered ferromagnetic alloy Ni-V revealed with small angle neutron scattering, *AIP Adv.* **10**, 015036 (2020).
- [49] D. Olds, C. N. Saunders, M. Peters, T. Proffen, J. Neuefeind, and K. Page, Precise implications for real-space pair distribution function modeling of effects intrinsic to modern time-of-flight neutron diffractometers, *Acta Crystallogr. A* **74**, 293 (2018).
- [50] R. Radebaugh and P. H. Keesom, Low-temperature thermodynamic properties of vanadium. I. Superconducting and normal states, *Phys. Rev.* **149**, 209 (1966).
- [51] Q. Chen, Z. Huang, Z. Zhao, and C. Hu, First-principles study on the structural, elastic, and thermodynamics properties of Ni_3X (X: Al, Mo, Ti, Pt, Si, Nb, V, and Zr) intermetallic compounds, *Appl. Phys. A* **116**, 1161 (2014).
- [52] I. P. Gregory and D. E. Moody, The low temperature specific heat and magnetization of binary alloys of nickel with titanium, vanadium, chromium and manganese, *J. Phys. F* **5**, 36 (1975).